Computational Design of Proteins that Bind to TLR7 and FCyRII

Charlie Clarke

A thesis

submitted in partial fulfillment of the

requirements for the degree of

Master of Science

University of Washington

2023

Committee:

Neil King

Frank DiMaio

Program Authorized to Offer Degree:

Biochemistry

University of Washington

Abstract

Computational Design of Proteins that Bind to TLR7 and FCyRII

Charlie Clarke

Chair of the Supervisory Committee:

Neil King

Department of Biochemistry

TLR7 and FCyRIIa are common immune targets for adjuvant design because they elicit increased activation in TH1 and phagocytosis respectively. With the new wave of computational design tools including RF Diffusion, ProteinMPNN, and Alphafold 2, designing protein adjuvants for these targets has become possible. The results of the TLR7 adjuvant design campaign show through yeast display and BLI that there are 2 potential binding candidates. The IL6 activation assay showed that random arrangement of the binders was insufficient to trigger TLR7 signaling. The FCyRIIa initial campaign showed that the binders were incapable of differentiating between FCyRIIa and FCyRIIb/c. After adapting the current tools to account for a two state binding method in ProteinMPNN, the set of binders was capable of differentiating between FCyRIIa and FCyRIIb/c in Alphafold2.

Acknowledgements

I would like to start by thanking everyone in the King Lab, but especially Chloe Adams for training me in the wet lab and developing the first round of FCyRII binders, Cameron Criswell for teaching me everything I know about coding, Lieselotte Kreuk for testing all of the FCyRII mini-binders *in vivo*, and Neil King for his unwavering guidance throughout these projects. Finally, I would like to thank my wonderful partner Peter Davies for always believing I could accomplish anything I set out to.

Table of Contents

Chapter 1 Introduction

1. Introduction To Immune Adjuvants

Traditional vaccinations have historically consisted of live attenuated virus, heat killed virus, or natural infection to keep levels of circulating virus low in the population[1]. These methods were effective, albeit with an intolerably high mortality cost. Today the field of vaccine development has expanded to include subunit vaccines, which although easier to manufacture, and safer to administer can have waning protection as seen in the head to head comparison of the COVID-19 vaccines[2]. This observation is likely due to the exclusion of natural adjuvants: viral nucleic acids, proteins, and lipids. Adjuvants are required in subunit vaccines to replicate the protection seen in whole virus vaccinations. These adjuvants historically have been small molecules, mineral salts, or oil in water emulsions that are incapable of producing an equivalent immune response to natural infection[3]. An additional hurdle to incorporating these adjuvants is that they have not been shown to safely produce a TH1 response on their own due to systemic immune activation. Typically these adjuvants need to be displayed on a nanoparticle to induce a more localized, safer, and ultimately more effective response[4,5]. In the wake of mRNA vaccines traditional small molecule adjuvants are losing some utility because they cannot be coded into an RNA sequence for inclusion in the vaccinations.

The innate immune system has multiple methods of receptors that have evolved to sense pathogens by either binding them directly or by binding to natural or manufactured adjuvants. This thesis will focus on two such classes of receptors: fragment crystallizable binding receptors (FCRs) and toll-like receptors (TLRs). TLRs are anchored on the cell surface and in the endosome while FC receptors are always localized to the surface of cells. These two locations act as the early warning system for detecting intracellular and extracellular infection. It stands to

reason that if a vaccine is targeting a specific class of virus that it should be capable of eliciting the same response as the natural infection. To achieve this end, the adjuvants utilized have to be designed to activate the specific immunological receptors the virus would naturally activate.

2. TLR7: Role and Activation

TLR7 is an endosomal TLR responsible for sensing single stranded ribonucleic acid (ssRNA) and free floating guanosine nucleotides[7,8]. While still somewhat obfuscated, during natural infection it is likely that TLR7 is a key component of generating a productive immune response due to its ligands generating a protective TH1 response[4]. Currently, there are no FDA approved vaccines that target TLR7 for activation because upon administration the current small molecule activators have proven to create systemic immunological toxicity[9]. To date the most successful example of a TLR7 adjuvant takes a synthetic nanoparticle and decorates it with TLR7 small molecule agonists[5,6]. This platform showed that the nanoparticle was retained in the lymph nodes and the spleen, greatly reducing systemic toxicity and improving the halflife[5,6].

With the rise of subunit and mRNA vaccines, incorporating small molecule adjuvants into the formulation becomes either highly difficult or impossible. This discrepancy creates a niche for a protein based adjuvant that can be incorporated into these developing vaccine platforms. The current small molecule activators sit in between a TLR7 dimer and cause a dynamic change in the C-terminus of the protein to trigger signaling across the membrane[10]. Designing a protein to mimic this activation is complicated because of the size difference. A protein adjuvant that folds stably, even in its smallest form is likely to be an order of magnitude larger than a small molecule[11]. This size discrepancy makes it difficult or potentially impossible to fit a protein adjuvant into the binding pocket and trigger the C-terminal conformational shift. Triggering the activation of TLR7 is driven by a few competing hypotheses: the clustering

hypothesis argues that if you bring receptors into contact with each other in large clusters, they will start signaling due to bumping into their signaling partner in the correct conformation by chance[12]. The geometric hypothesis argues that each receptor has specific geometric constraints that must be satisfied before signaling can be triggered[10]. Digging into these two hypotheses is critical to designing a protein based adjuvant for TLR7.

3. FCyRIIa: Role and Activation

Fragment crystallizable receptor II a (FCyRIIa) is a low affinity cell surface receptor that binds to the FC portion of an IgG antibody and triggers phagocytosis by immune presenting cells[13]. This receptor is critical in linking the adaptive immune system to the innate immune system. When an antibody binds to its cognate antigen, macrophages and other antigen presenting cells use FC receptors to internalize antigens and mount the appropriate immunological response[14].

FCyRII has multiple isozymes that play different roles depending on their expression and cell type. FCyRIIa is an activating receptor expressed in some T cell subtypes, macrophages, monocytes, and neutrophils whereas FCyRIIb is a repressive receptor that is primarily differentially expressed on B cells[15]. Not much is known about the expression of FCyRIIc, but it is known to be an activating receptor[15]. FCyRIIb and FCyRIIc have identical ectodomains and different transmembrane and signaling domains[16]. The ectodomain FCyRIIb/c and FCyRIIa have a 85% identity with few amino acid mismatches[16]. These mismatches cause the two ectodomains to have different affinities to the FC region of certain antibodies[17]. To design a protein based adjuvant that specifically binds to FCyRIIa and not to FCyRIIb/c the amino acid mismatches need to be specifically targeted to provide enough contrast between the binding interfaces.

4. Computational Protein Design

Generating new proteins has long been pioneered in the Baker lab, with the first completely *de novo* protein generation occurring in 2015 with the alpha-helical tandem repeat proteins[18]. Over the years, as computing became faster and less expensive, new tools have come to the protein design space. The first wave of protein design was based on designing proteins that fold in expected ways by basing them off of known folds[18,19,20] and the second wave designed specific protein protein interactions[21]. The first step in generating *de novo* protein protein interactions starts with the identification of a high confidence structure and a potential binding site[22,23]. This identification was achieved through a combination of methods. First, the potential structures were inspected for high confidence regions and poorly resolved or flexible regions[22,23]. Then each individual residue of the molecule was scored based on its hydrophobicity which remains the most predictive way to date to design a successful protein protein interaction[22,23]. When looking at an exposed hydrophobic region the more exposed residues the higher potential the binding site, but typically 2-3 exposed hydrophobic residues is the minimum acceptable amount[22,23]. After hydrophobic regions were picked, all of the flexible hydrophobic regions were eliminated. Next, a patch of surface residues were selected and passed through the Rifgen computational method that generates all of the possible side chain rotamers for the desired binding patch. In parallel, we also needed to determine the optimal shape complementarity between the designed protein and the target through the Patchdock method, which takes a library of mini-proteins with random sequences and places them onto the target[22,23]. The placement process generates patches of coverage where the mini-protein could sit. In the next step the Rifdock method combined the outputs of the generated side chain rotamers and the complementarity of the mini-proteins to find the best patches for the possible side chain positions[22,23]. The mini-proteins with the best complementarity were then sent through

ProteinMPNN, a message passing neural network that optimizes the side chain residues for the mini-protein to become a mini-binder[24]. The final step in this process is to fold all of the designed complexes through Alphafold2 (AF2) and score the complex by the predicted aligned error (PAE) of interaction, see Figure 1 for a visual overview of the design pipeline[25]. The lower the score the better the more likely the binder is to fold and bind the way that AF2 predicted it to[25].

Currently, Rifgen, Patchdock, and Rifdock have all been replaced by a new method RFDiffusion. This method rapidly generates new mini-protein backbones through utilization of a denoising diffusion probabilistic model that generates photorealistic images in response to text prompts[26]. The initial image is corrupted with Gaussian noise and is then denoised back into a 3D object. This in combination with deep learning models such as AF2, allow the generated 3D models to form specific folds[26]. The method is such that the user tells the program the required parameters such as hotspot residues, number of generated structures, size of the structures, and the number of denoising steps, then 3D models are generated to fit the parameters[26]. Diffusion can also take existing mini-binders and pass them through an additional method called partial diffusion that is currently unpublished. Partial diffusion can take a mini-binder that doesn't bind well, and make slight alterations to the backbone and positioning on the target by adding gaussian noise and denoising in smaller timesteps. Then the outputs are fed back through Protein MPNN and AF2 to generate the sequence and test the binding interface. Combined these three methods have paved the way for a golden age of protein design.

Chapter 2 TLR7 Design Results

1. TLR7 Binder Design: Clustering Hypothesis

In the first design campaign for a TRL7 binder, five potential sites were selected for their hydrophobicity and distance from glycosylation sites see Figure 2 and Table 1. Three sites were positioned on the interior face and two sites were positioned on the exterior face. These five sites were put through the original protein-protein design pipeline laid out previously. After running Rifgen, Patchdock, Rifdock, ProteinMPNN, and AF2 18,000 designs were considered to have passing scores. Of those 18,000 designs, the mini-binders predicted to bind to the interior face of the protein appeared to have far fewer predicted binders than the exterior face binders, likely due to steric clashes.

2. Yeast Display Screening

These designs were ordered on a chip with unique forward and reverse primers and were transformed into a yeast display platform. This platform uses an SCGAA induction system to express the mini-binder attached to the surface of the yeast cell with a linker that includes a c-myc tag. This two part system allows for the protein expression and protein binding to be confirmed by FACS sorting through fluorescein isothiocyanate (FITC) and Streptavidin R-Phycoerythrin Conjugate (SAPE) fluorescence. The first 2 rounds of FACS sorting revealed enrichment of FITC/SAPE +/+ cells, see Figure 3 A-C. These cells were collected and plated for colony PCR and isolated colony sorting. Isolated Colony sorting revealed that there was binding present as low as 7.8nM of receptor while controlling for avidity, see Figure 3 D. Colony PCR was performed and it was discovered that all of the colonies tested belonged to 1 binder.

3. Biolayer Interferometry: Binding to hTLR7

That design was expressed in pET28b with a 6xHIS tag and tested by biolayer interferometry (BLI) to confirm binding see Figure 4. The BLI showed binding as low as 1.88nM at pH 7.4, see Figure 4A. Binding was then tested again at pH 5.5 to assess binding at an

endosomal pH, and showed binding as low as 3.75nM, see Figure 4B. To test the clustering hypothesis, the I53-50 nanoparticle was then used as the basic display platform. This two component nanoparticle expresses well in E.coli and assembles quickly and reliably when component A is mixed with component B. The mini-binder was designed and expressed with a flexible 12xGS linker attaching it to the N terminal end of I53-50A. The nanocage was retested for binding at pH 7 and pH 5.5 and showed tighter binding than free mini-binder, consistent with avidity, see Figure 4C-D.

4. IL6 Activation Testing

Activation of TLR7 was then measured through a peripheral blood mononuclear cell (PBMC) assay developed by Maggie Ahlrichs and me. When TLR7 is activated the cells secrete IL6 and the levels of IL6 can be tested by an anti-IL6 enzyme-linked immunosorbent assay (ELISA). Polymyxin B sulfate was used in this assay to neutralize any residual endotoxin leftover from purifying the nanoparticle components out of E. coli. The PBMC cells were incubated with Resiquimod (R848), mini-binder I53-50 fusion with polymyxin sulfate B, and the mini-binder I53-50 fusion without polymyxin B sulfate for 6 hours at which point the cells were spun down. The supernatant was removed and tested by ELISA. When incubated with R848 the cells showed sigmoidal activation, see Figure 5A. When incubated with the mini-binder I53-50 fusion without polymyxin B sulfate there was linear activation, see Figure 5B. When incubated with the mini-binder nanoparticle fusion with polymyxin B sulfate there was no activation, see Figure 5B.

5. Second Design Campaign: Geometric Hypothesis

When the nanoparticle display failed, my hypothesis turned towards accounting for the specific geometry of TLR7 activation and designing a molecule that will pull the dimer into its

active conformation. I used the RF Diffusion method to pursue 2 design campaigns. The first was focused on developing a new mini-binder, to the exterior face of TLR7 monomer on the C-terminal half of the ectodomain. This way this new mini-binder could be joined to the original binder to fuse them into one activating protein with a linker to specifically pull the ectodomains into the active conformation. The second was focused on designing a binder at the interface of 2 TLR7 monomers at the guanosine binding site. The first new design campaign had 2 usable outputs with a pAE under 15, likely due to the binding site not having much access to exposed hydrophobics Figure 6A. Of those 2 designs, one of them showed binding at 1uM and down to 250nM at pH 7.4, see Figure 6B. The second campaign is currently half completed. These designs were created to fit between the active TLR7 dimer, see Figure 7A. There were 8,838 binders generated and 271 with a pAE under 15, however most of the binders are so small they likely would not fold with high fidelity, see Figure 7B. For these designs to be ordered the pLDDT of folding needs to be over 80 and currently only one has a pLDDT of >80 Figure 7C.

Chapter 3 FCyRIIa Design Results

1. Previous Work and Collaboration: Non-Specific FCyRII Binder

Previous work in the lab, designed and identified 8 mini-binders that could selectively bind to FCyRII. I was able to express 4 of these mini-binders and show that MB5 bound to both FCyRIIa and FCyRIIb/c, see Figure 8A. That mini-binder was shown by a collaborator to preliminarily bind to macrophages on ice, see Figure 8B. Then the collaborators designed a tissue assay to test if the MB5 mini-binder could promote clearance of bacteria in a tissue assay. In this assay, the tissue culture was infected with *A. baumannii* and the fluorescent beads were used to bring FCyRII binding cells into contact with the bacterium. In their experiments, the MB5 protein promoted clearance of the bacterium over B1gp45 alone in vitro and in vivo 8

hours post injection. Figure 8C-E. While this mini-binders was not capable of differentiating between FCyRIIa and FCyRIIb/c, it still shows adjuvant potential, and the potential of a specific FCyRIIa binder.

2. Initial Design Campaign: Classic Method

To differentiate between FCyRIIa and FCyRIIb/c, I started by mapping all of the surface exposed amino acid mismatches and identified areas of the ectodomain that were enriched with surface exposed mismatches see Figure 9A and Table 2. The 2 sites with the most distinct mismatches focused on Site A (M104V, H131R, L132S, and T135N) and Site B (Q127K and H131R). RF Diffusion was used to generate 200 structures to these sites. Of those 200, 13 were selected for their complementarity and partially diffused. Then partial diffusion was used to expand that pool of binders to 3,250. Protein MPNN generated 2 sequences for each of those binders, and finally they were scored by AF2. Of those 6,500 binders, none had a PAE under 15 and was specific to FCyRIIa and not FCyRIIb/c see Table 3.

3. Development of Two State Binder Tools

Another lab member created a helper script for ProteinMPNN that allows you to specify that you want sequence outputs to bind to one receptor and not another. Originally it was created for cage design, but I repurposed the code for two state mini-binder design. To use this piece of script in the normal binder design process, the outputs of each stage needed to be manipulated in specific ways to be compatible. To prepare the RF Diffusion outputs for the ProteinMPNN helper script, the mini-binder must be duplicated in the PDB and the negative binding partner is added. This negative pair is then translated 1000 angstroms away so that there is no confusion about which mini-binder is paired with which receptor. Then, the Protein MPNN flags can be modified to tell the program to keep the sequence the same for both mini-binders, set the binding

specificity from +1 to -1 for each receptor, and output the sequences. Once those sequences are generated they are threaded over the original diffusion outputs and run through AF2.

4. Second Design Campaign: Two State Method

The initial RF Diffusion generated 250 outputs 13 of which were capable of folding and in the correct orientation. Those 13 outputs generated 3,250 partial diffusion outputs. Those partial diffusion outputs generated 52,000 Protein MPNN sequences. Those ProteinMPNN sequences generated 209 AF2 outputs with pAE under 15 for FCyRIIa and PAE > 20 FCyRIIb/c see Table 2. Not all of the design sites were equally successful and a majority of the binders came from Site A, see Figure 9A where there are multiple mismatched amino acids with high contrast. The best design by far was design 143 which generated 187 binders with a pAE under 15, see Figure 9B.

Chapter 4 Conclusions

1. TLR7 Future Directions: Structural Activation

Protein based activation of TLR7 remains elusive for now. It is possible that the clustering hypothesis can still be confirmed if the linker length from the nanocage was either too short or too long, but it appears likely that the specific geometric constraints must be satisfied by the designed adjuvant. As the methods for RFDiffusion continue to expand and become fully realized, it is likely that designing to areas previously off the table will become available. The next step in this project will likely need to include designing binders to less hydrophobic sites, designing binders to glycosylation shielded hydrophobic sites, or even designing a binder to fit in the guanosine binding pocket. In the meantime, the current binder can be labeled and used to visualize the localization of the N-terminal half of TLR7. It would be interesting to use the

current binder to probe whether the N-terminal and C-terminal half of TLR7 stay associated after cleavage of the Z-loop under different activation conditions.

2. FCyRIIa Future Directions: Potential Binders

Our collaborators showed that by binding the FCyRII receptors with our minibinders we are able to increase the molecule's internalization and clearance. Hopefully by designing to a site that can differentiate between FCyRIIa and FCyRIIb/c we can more specifically tune the immune response and potentially see increased rates of internalization. This second phase of minibinders has a lot of promise to specifically target FCyRIIa and with the libraries already created, the next step is to order and test the best designs before handing the specific binders off to our collaborators.

3. Two State Script Capabilities

Finally, the script I created to carry out the two state design process, has the capability to be used for both +/- binding as well as +/+ or -/- binding. One of the larger hurdles we have had in the binder design process is designing for both mouse and human isoforms so that the binder can be tested in the mouse model system. This script has the capability to design binders that will bind in the same location to both isoforms. The major caveat is that both targets must have relatively few mismatches in the binding pocket for ProtienMPNN to be able to design a sequence that will bind both. Hopefully this script will continue to be useful for making cross reactive and specifically reactive binders in future projects.

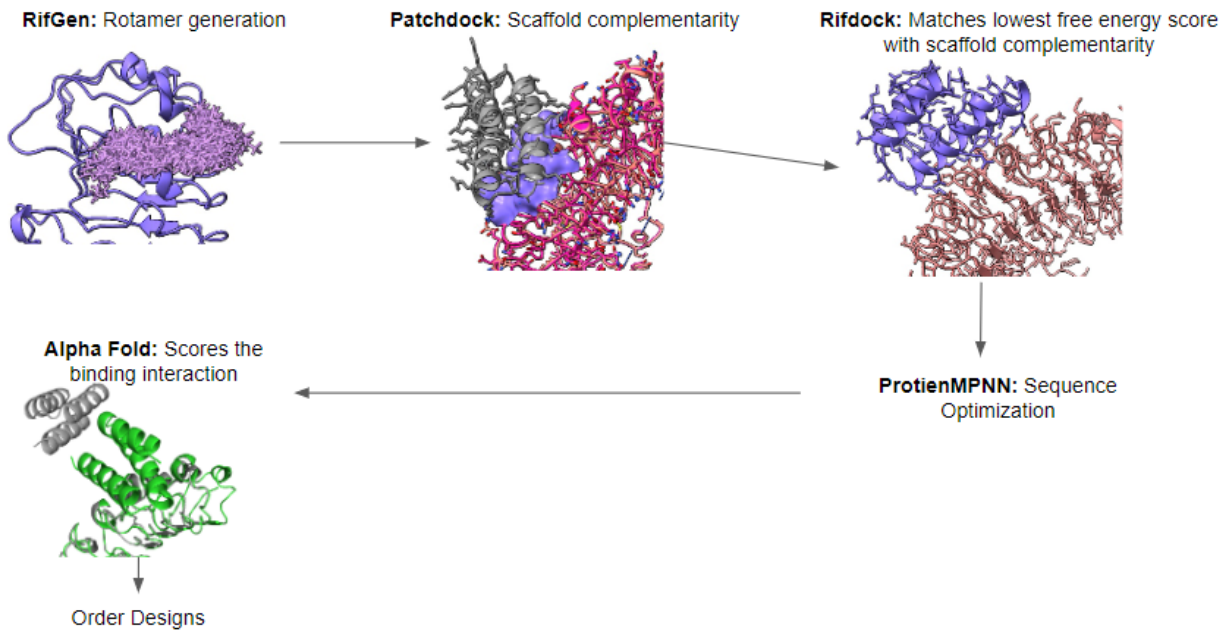

Figure 1. Diagram of the mini-binder design process. RifGen, Patchdock, Rifdock, ProteinMPNN, Alphafold2

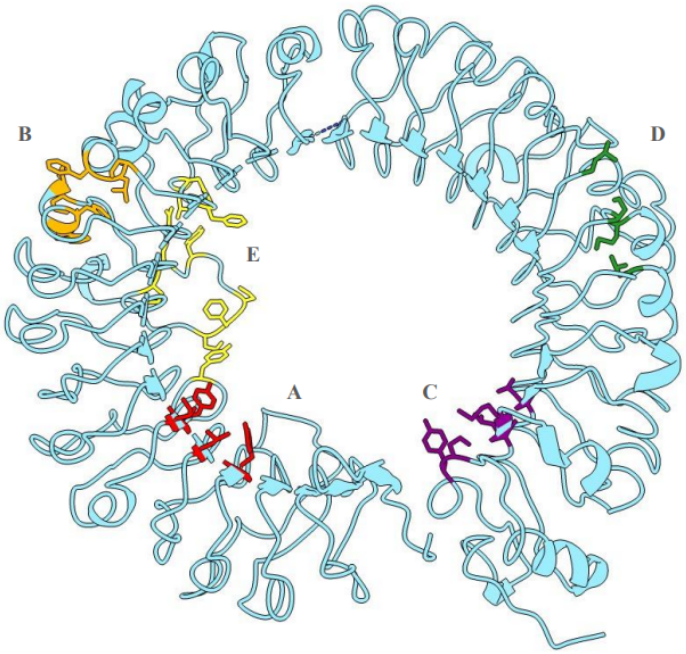

Figure 2. Structure of hTLR7 (RCSB:7CYN) with initial design sites highlighted. Site A in Red, Site B in Orange, Site C in Purple, Site D in Green, Site E in Yellow.

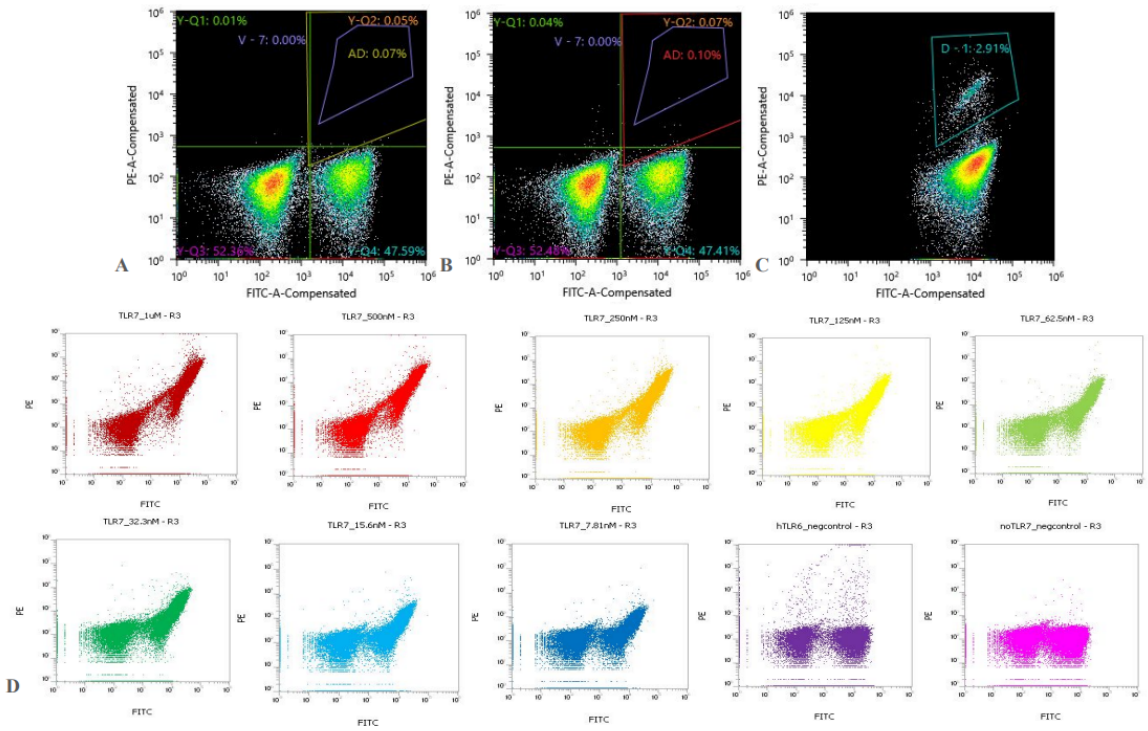

Figure 3. FITC/SAPE +/+ initial sorting 1uM hTLR7 of the yeast display library. Negative control without receptor 2A. Consecutive sorts both 1uM hTLR7 2B-2C. Isolated colony sort with decreasing receptor starting at 1uM and decreasing to 7.81nM 2D.

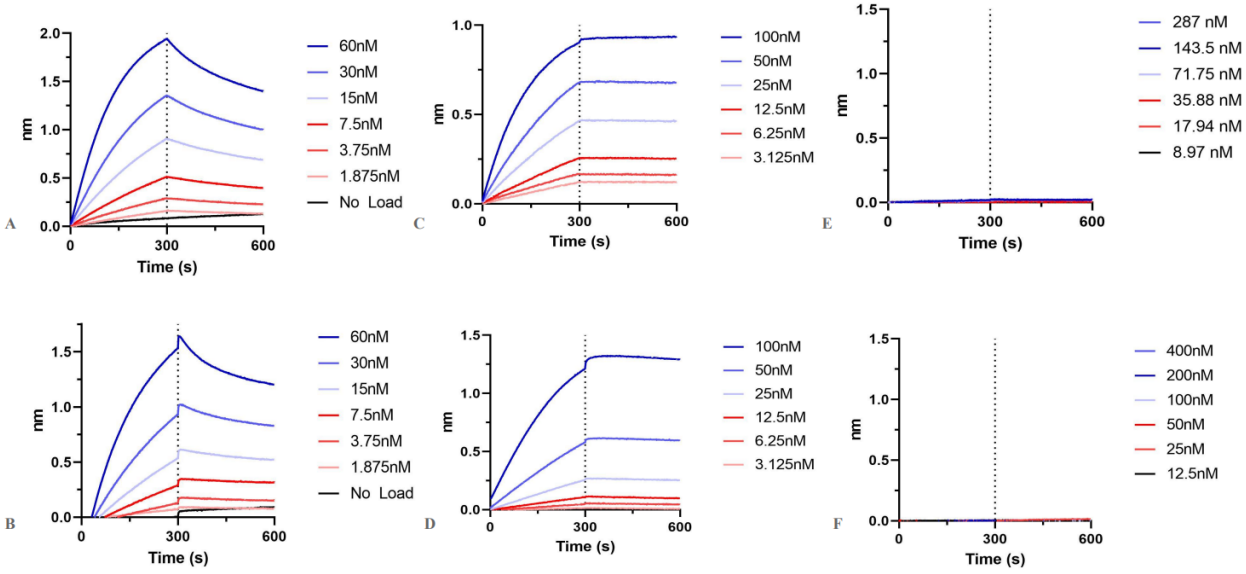

Figure 4. Biolayer interferometry testing of TLR7 to unbound mini-binder at pH 7.4 and 5.5 (4A,4B), mini-binder I53-50 nanoparticle pH 7.4 and 5.5(4C,4D), mini-binder against TLR6 at pH 7.4 (4E), and a mini-binder specific to TLR2 against TLR7 at pH 7.4 (4F).

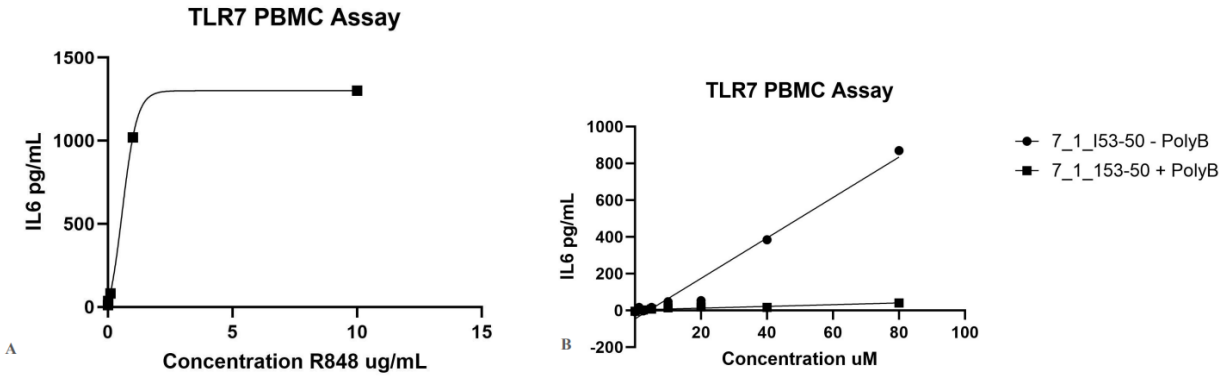

Figure 5. IL6 concentration of human PBMC assay after 6 hour incubation at 37ºC. R848 sigmoidal secretion of IL6 (5A). Mini-binder I53-50 fusion linear secretion of IL6 with and without polymyxin B sulfate (5B).

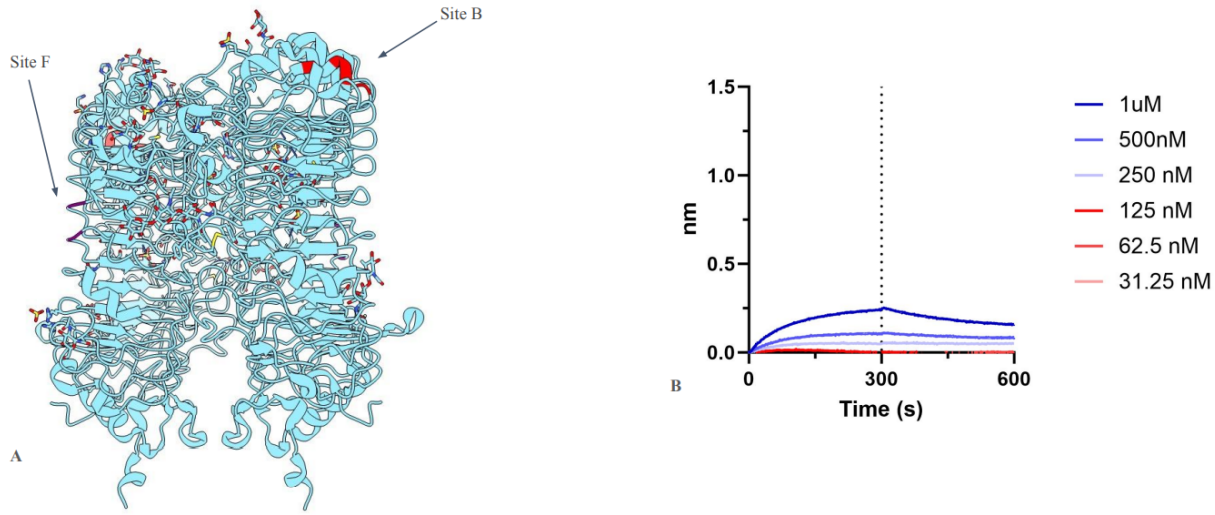

Figure 6. Diagram of design site F in relation to site B where the current mini-binder is hypothesized to bind (6A). Biolayer interferometry of the one site F binder at decreasing concentrations of hTLR7 (6B).

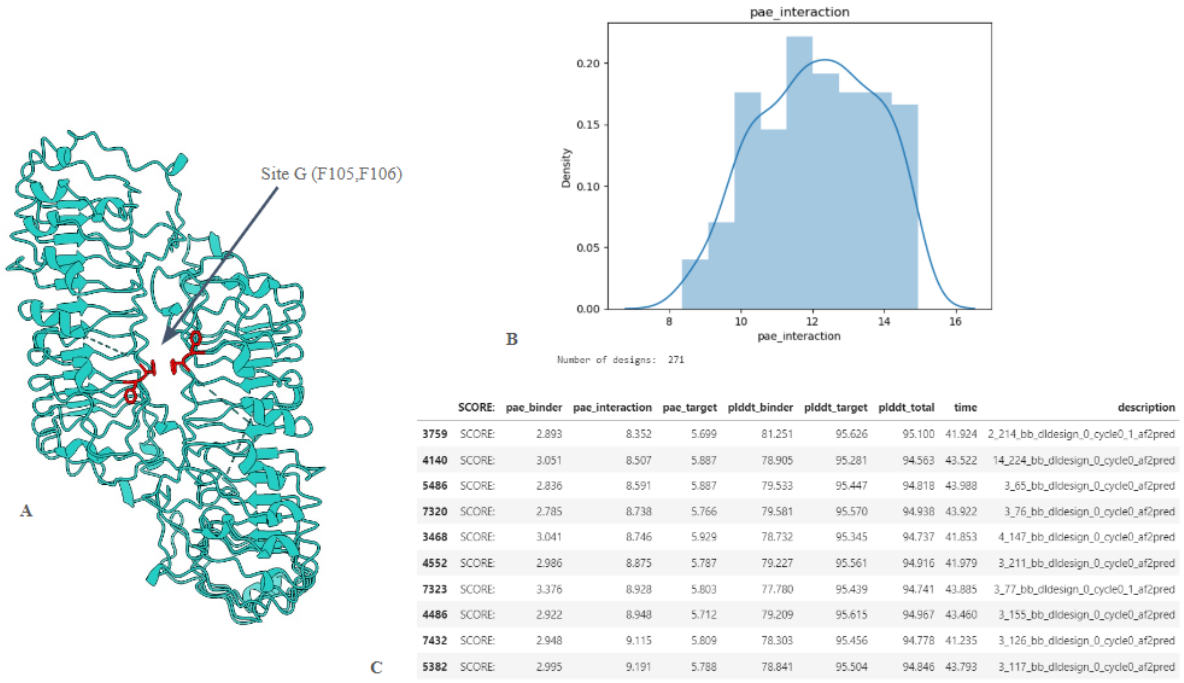

C

	SCORE:	pae_binder	pae_interaction	pae_target	plddt_binder	plddt_target	plddt_total	time	description
3759	SCORE:	2.893	8.352	5.699	81.251	95.626	95.100	41.924	2_214_bb_dldesign_0_cycle0_1_af2pred
4140	SCORE:	3.051	8.507	5.887	78.905	95.281	94.563	43.522	14_224_bb_dldesign_0_cycle0_af2pred
5486	SCORE:	2.836	8.591	5.887	79.533	95.447	94.818	43.988	3_65_bb_dldesign_0_cycle0_af2pred
7320	SCORE:	2.785	8.738	5.766	79.581	95.570	94.938	43.922	3_76_bb_dldesign_0_cycle0_af2pred
3468	SCORE:	3.041	8.746	5.929	78.732	95.345	94.737	41.853	4_147_bb_dldesign_0_cycle0_af2pred
4552	SCORE:	2.986	8.875	5.787	79.227	95.561	94.916	41.979	3_211_bb_dldesign_0_cycle0_af2pred
7323	SCORE:	3.376	8.928	5.803	77.780	95.439	94.741	43.885	3_77_bb_dldesign_0_cycle0_1_af2pred
4486	SCORE:	2.922	8.948	5.712	79.209	95.615	94.967	43.460	3_155_bb_dldesign_0_cycle0_af2pred
7432	SCORE:	2.948	9.115	5.809	78.303	95.456	94.778	41.235	3_126_bb_dldesign_0_cycle0_af2pred
5382	SCORE:	2.995	9.191	5.788	78.841	95.504	94.846	43.793	3_117_bb_dldesign_0_cycle0_af2pred

Figure 7. Diagram of design site G: a top down view of the activated dimer and the diffusion hotspot residues colored in red (7A). Histogram of potential binders that have a pAE of binding under 15 (7B). Individual mini-binder score outputs showing the explicit pAE's of interaction and pLDDT of binder and target(7C).

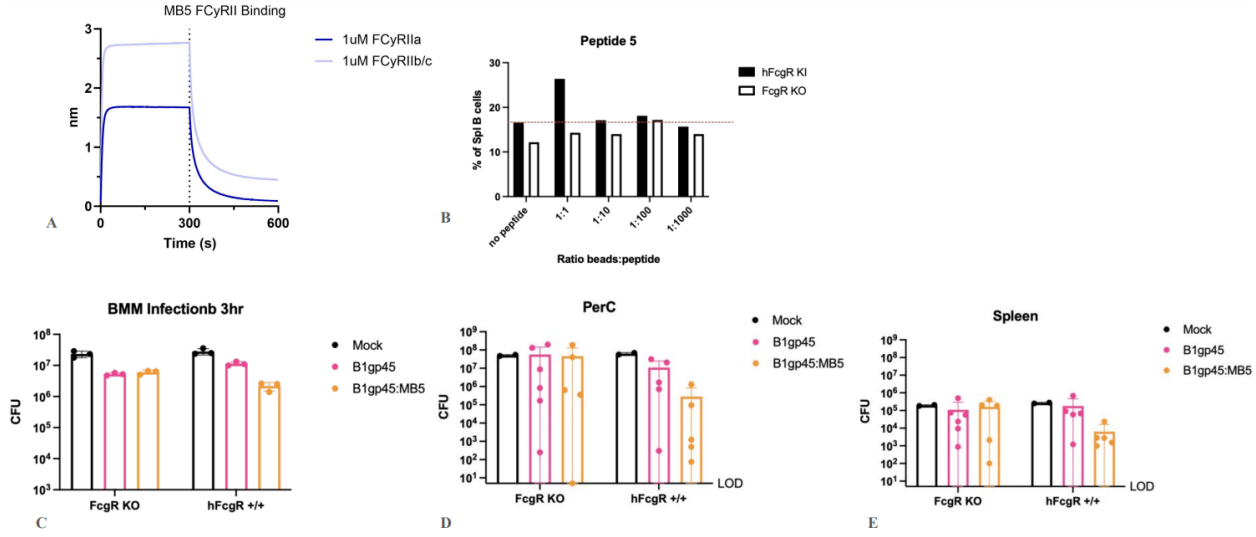

Figure 8. Biolayer interferometry data of MB5 to 1uM FCyRIIa and FCyRIIb/c (8A). Percentage of splenocyte B-cells bound to MB5 decorated fluorescent bead in hFCyR knockin and FCyR knockout mice (8B). Clearance of *A. baumannii* by macrophages with addition of MB5/B1gp45 +/+ beads *in vitro* tissue culture (8C). Clearance of *A. baumannii* by macrophages with addition of MB5/B1gp45 +/+ beads *in vivo* 8 hours post infection in the peritoneal cavity

(8D). Clearance of *A. baumannii* by macrophages with addition of MB5/B1gp45 +/+ beads *in vivo* 8 hours post infection in the spleen (8E).

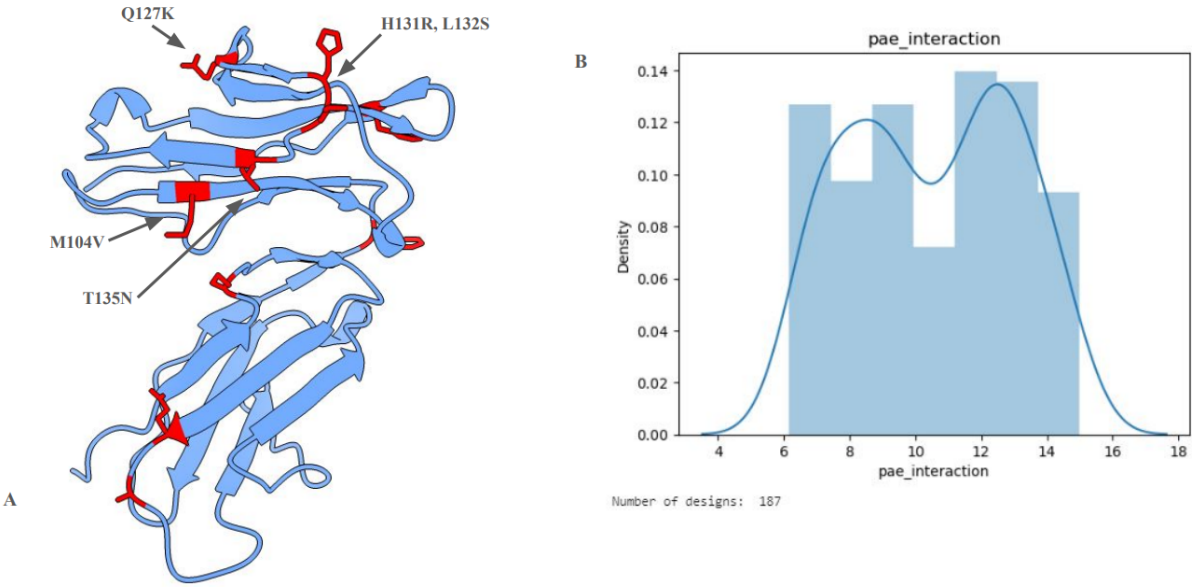

Figure 9. Diagram of FCyRIIa with FCyRIIb/c mismatches highlighted in red and key mutations labeled (9A). Design 143 histogram of two state binders that bind exclusively to FCyRIIa (9B).

Site A	Site B	Site C	Site D	Site E	Site F	Site G
Y103	P276	Y673	L572	Y155	L650	Chain A F105
L122	P277	M699	M595	P231	P675	Chain A F106
I147	W279	L701	P597	R323		Chain B F105
Y148	F280	P728	L620	Y234		Chain B F106
Y407	F308	Y729		P237		
	L309			F238		
	P310			P239		
				F319		
				F321		
				L323		

Table 1. List of target residues for all rounds of TLR7 design Sites A-G.

Mutations
P12Q
Q27R
A29T
F85S
M104V
Q127K
H131R

L132S
T135N
F160Y

Table 2. List of solvent exposed residue mismatches between FCyRIIa and FCyRIIb/c.

	First Design Pathway		**Two State Design Pathway**	
Design Stage	Outputs per Structure	Total Outputs	Outputs per Structure	Total Outputs
Diffusion	200	13	200	13
Partial Diffusion	250	3250	250	3250
ProteinMPNN	2	6500	16	52000
AF2	6500	0	52000	209

Table 3. Classical design pathway outputs showing the number of output structures per stage and total usable outputs at each stage showing no usable outputs after AF2 vs. the two state design pathway showing 209 usable outputs after AF2.

References

1. Francis MJ. Recent Advances in Vaccine Technologies. Vet Clin North Am Small Anim Pract. 2018 Mar;48(2):231-241. doi: 10.1016/j.cvsm.2017.10.002. Epub 2017 Dec 6. PMID: 29217317; PMCID: PMC7132473.
2. Rotshild V, Hirsh-Raccah B, Miskin I, Muszkat M, Matok I. Comparing the clinical efficacy of COVID-19 vaccines: a systematic review and network meta-analysis. Sci Rep. 2021 Nov 23;11(1):22777. doi: 10.1038/s41598-021-02321-z. PMID: 34815503; PMCID: PMC8611039.

3. Facciolà A, Visalli G, Laganà A, Di Pietro A. An Overview of Vaccine Adjuvants: Current Evidence and Future Perspectives. Vaccines (Basel). 2022 May 22;10(5):819. doi: 10.3390/vaccines10050819. PMID: 35632575; PMCID: PMC9147349.
4. https://doi.org/10.1111/j.0105-2896.2004.00144.x
5. Yin, Q., Luo, W., Mallajosyula, V. et al. A TLR7-nanoparticle adjuvant promotes a broad immune response against heterologous strains of influenza and SARS-CoV-2. Nat. Mater. 22, 380–390 (2023). https://doi.org/10.1038/s41563-022-01464-2
6. Lynn GM, Laga R, Darrah PA, Ishizuka AS, Balaci AJ, Dulcey AE, Pechar M, Pola R, Gerner MY, Yamamoto A, Buechler CR, Quinn KM, Smelkinson MG, Vanek O, Cawood R, Hills T, Vasalatiy O, Kastenmüller K, Francica JR, Stutts L, Tom JK, Ryu KA, Esser-Kahn AP, Etrych T, Fisher KD, Seymour LW, Seder RA. In vivo characterization of the physicochemical properties of polymer-linked TLR agonists that enhance vaccine immunogenicity. Nat Biotechnol. 2015 Nov;33(11):1201-10. doi: 10.1038/nbt.3371. Epub 2015 Oct 26. PMID: 26501954; PMCID: PMC5842712.
7. Shibata T, Ohto U, Nomura S, Kibata K, Motoi Y, Zhang Y, Murakami Y, Fukui R, Ishimoto T, Sano S, Ito T, Shimizu T, Miyake K. Guanosine and its modified derivatives are endogenous ligands for TLR7. Int Immunol. 2016 May;28(5):211-22. doi: 10.1093/intimm/dxv062. Epub 2015 Oct 20. PMID: 26489884; PMCID: PMC4888345.
8. Lund JM, Alexopoulou L, Sato A, Karow M, Adams NC, Gale NW, Iwasaki A, Flavell RA. Recognition of single-stranded RNA viruses by Toll-like receptor 7. Proc Natl Acad Sci U S A. 2004 Apr 13;101(15):5598-603. doi: 10.1073/pnas.0400937101. Epub 2004 Mar 19. PMID: 15034168; PMCID: PMC397437.

9. Lu R, Groer C, Kleindl PA, Moulder KR, Huang A, Hunt JR, Cai S, Aires DJ, Berkland C, Forrest ML. Formulation and preclinical evaluation of a toll-like receptor 7/8 agonist as an anti-tumoral immunomodulator. J Control Release. 2019 Jul 28;306:165-176. doi: 10.1016/j.jconrel.2019.06.003. Epub 2019 Jun 4. PMID: 31173789; PMCID: PMC6679596.
10. Tojo, S., Zhang, Z., Matsui, H. et al. Structural analysis reveals TLR7 dynamics underlying antagonism. Nat Commun 11, 5204 (2020). https://doi.org/10.1038/s41467-020-19025-z
11. Bhardwaj, G., Mulligan, V., Bahl, C. et al. Accurate de novo design of hyperstable constrained peptides. Nature 538, 329–335 (2016). https://doi.org/10.1038/nature19791
12. Li M, Yu Y. Innate immune receptor clustering and its role in immune regulation. J Cell Sci. 2021 Feb 17;134(4):jcs249318. doi: 10.1242/jcs.249318. PMID: 33597156; PMCID: PMC7904094.
13. Junker F, Gordon J, Qureshi O. Fc Gamma Receptors and Their Role in Antigen Uptake, Presentation, and T Cell Activation. Front Immunol. 2020 Jul 3;11:1393. doi: 10.3389/fimmu.2020.01393. PMID: 32719679; PMCID: PMC7350606.
14. Fitzer-Attas CJ, Lowry M, Crowley MT, Finn AJ, Meng F, DeFranco AL, Lowell CA. Fcgamma receptor-mediated phagocytosis in macrophages lacking the Src family tyrosine kinases Hck, Fgr, and Lyn. J Exp Med. 2000 Feb 21;191(4):669-82. doi: 10.1084/jem.191.4.669. PMID: 10684859; PMCID: PMC2195832.
15. Anania JC, Chenoweth AM, Wines BD, Hogarth PM. The Human FcγRII (CD32) Family of Leukocyte FcR in Health and Disease. Front Immunol. 2019 Mar 19;10:464. doi: 10.3389/fimmu.2019.00464. PMID: 30941127; PMCID: PMC6433993.

16. Qiu WQ, de Bruin D, Brownstein BH, Pearse R, Ravetch JV. Organization of the human and mouse low-affinity Fc gamma R genes: duplication and recombination. Science. 1990 May 11;248(4956):732-5. doi: 10.1126/science.2139735. PMID: 2139735.
17. Nagelkerke SQ, Schmidt DE, de Haas M, Kuijpers TW. Genetic Variation in Low-To-Medium-Affinity Fcγ Receptors: Functional Consequences, Disease Associations, and Opportunities for Personalized Medicine. Front Immunol. 2019 Oct 3;10:2237. doi: 10.3389/fimmu.2019.02237. PMID: 31632391; PMCID: PMC6786274.
18. Doyle, L., Hallinan, J., Bolduc, J. et al. Rational design of α-helical tandem repeat proteins with closed architectures. Nature 528, 585–588 (2015). https://doi.org/10.1038/nature16191
19. Koday MT, Nelson J, Chevalier A, Koday M, Kalinoski H, Stewart L, Carter L, Nieusma T, Lee PS, Ward AB, Wilson IA, Dagley A, Smee DF, Baker D, Fuller DH. A Computationally Designed Hemagglutinin Stem-Binding Protein Provides In Vivo Protection from Influenza Independent of a Host Immune Response. PLoS Pathog. 2016 Feb 4;12(2):e1005409. doi: 10.1371/journal.ppat.1005409. PMID: 26845438; PMCID: PMC4742065.
20. Boyken SE, Chen Z, Groves B, Langan RA, Oberdorfer G, Ford A, Gilmore JM, Xu C, DiMaio F, Pereira JH, Sankaran B, Seelig G, Zwart PH, Baker D. De novo design of protein homo-oligomers with modular hydrogen-bond network-mediated specificity. Science. 2016 May 6;352(6286):680-7. doi: 10.1126/science.aad8865. Erratum in: Science. 2016 May 20;352(6288). pii: aag1318. doi: 10.1126/science.aag1318. PMID: 27151862; PMCID: PMC5497568.

21. Bryan CM, Rocklin GJ, Bick MJ, Ford A, Majri-Morrison S, Kroll AV, Miller CJ, Carter L, Goreshnik I, Kang A, DiMaio F, Tarbell KV, Baker D. Computational design of a synthetic PD-1 agonist. Proc Natl Acad Sci U S A. 2021 Jul 20;118(29):e2102164118. doi: 10.1073/pnas.2102164118. PMID: 34272285; PMCID: PMC8307378.
22. Cao L, Coventry B, Goreshnik I, Huang B, Sheffler W, Park JS, Jude KM, Marković I, Kadam RU, Verschueren KHG, Verstraete K, Walsh STR, Bennett N, Phal A, Yang A, Kozodoy L, DeWitt M, Picton L, Miller L, Strauch EM, DeBouver ND, Pires A, Bera AK, Halabiya S, Hammerson B, Yang W, Bernard S, Stewart L, Wilson IA, Ruohola-Baker H, Schlessinger J, Lee S, Savvides SN, Garcia KC, Baker D. Design of protein-binding proteins from the target structure alone. Nature. 2022 May;605(7910):551-560. doi: 10.1038/s41586-022-04654-9. Epub 2022 Mar 24. PMID: 35332283; PMCID: PMC9117152.
23. Cao L, Goreshnik I, Coventry B, Case JB, Miller L, Kozodoy L, Chen RE, Carter L, Walls AC, Park YJ, Strauch EM, Stewart L, Diamond MS, Veesler D, Baker D. De novo design of picomolar SARS-CoV-2 miniprotein inhibitors. Science. 2020 Oct 23;370(6515):426-431. doi: 10.1126/science.abd9909. Epub 2020 Sep 9. PMID: 32907861; PMCID: PMC7857403.
24. Dauparas J, Anishchenko I, Bennett N, Bai H, Ragotte RJ, Milles LF, Wicky BIM, Courbet A, de Haas RJ, Bethel N, Leung PJY, Huddy TF, Pellock S, Tischer D, Chan F, Koepnick B, Nguyen H, Kang A, Sankaran B, Bera AK, King NP, Baker D. Robust deep learning-based protein sequence design using ProteinMPNN. Science. 2022 Oct 7;378(6615):49-56. doi: 10.1126/science.add2187. Epub 2022 Sep 15. PMID: 36108050;

25. Jumper J, Evans R, Pritzel A, Green T, Figurnov M, Ronneberger O, Tunyasuvunakool K, Bates R, Žídek A, Potapenko A, Bridgland A, Meyer C, Kohl SAA, Ballard AJ, Cowie A, Romera-Paredes B, Nikolov S, Jain R, Adler J, Back T, Petersen S, Reiman D, Clancy E, Zielinski M, Steinegger M, Pacholska M, Berghammer T, Bodenstein S, Silver D, Vinyals O, Senior AW, Kavukcuoglu K, Kohli P, Hassabis D. Highly accurate protein structure prediction with AlphaFold. Nature. 2021 Aug;596(7873):583-589. doi: 10.1038/s41586-021-03819-2. Epub 2021 Jul 15. PMID: 34265844; PMCID: PMC8371605.PMCID: PMC9997061.
26. Watson JL, Juergens D, Bennett NR, Trippe BL, Yim J, Eisenach HE, Ahern W, Borst AJ, Ragotte RJ, Milles LF, Wicky BIM, Hanikel N, Pellock SJ, Courbet A, Sheffler W, Wang J, Venkatesh P, Sappington I, Torres SV, Lauko A, De Bortoli V, Mathieu E, Ovchinnikov S, Barzilay R, Jaakkola TS, DiMaio F, Baek M, Baker D. De novo design of protein structure and function with RFdiffusion. Nature. 2023 Aug;620(7976):1089-1100. doi: 10.1038/s41586-023-06415-8. Epub 2023 Jul 11. PMID: 37433327; PMCID: PMC10468394.